Journal of Alloys and Compounds 495 (2010) 126–130

Contents lists available at ScienceDirect

Journal of Alloys and Compounds

journal homepage: www.elsevier.com/locate/jallcom

Preparation and characterization of ZnO transparent semiconductor thin films by sol–gel method

Chien-Yie Tsay[a,*], Kai-Shiung Fan[a], Sih-Han Chen[a], Chia-Hao Tsai[b]

[a] Department of Materials Science and Engineering, Feng Chia University, Taichung 407, Taiwan, ROC
[b] Research Alliance, Taiwan TFT LCD Association (TTLA), Hsinchu 310, Taiwan, ROC

ARTICLE INFO

Article history:
Received 22 October 2009
Received in revised form 20 January 2010
Accepted 21 January 2010
Available online 1 February 2010

Keywords:
Transparent oxide semiconductors
ZnO
Thin film
Sol–gel method
Optical properties

ABSTRACT

Transparent semiconductor thin films of zinc oxide (ZnO) were deposited onto alkali-free glass substrates by the sol–gel method and spin-coating technique. In this study, authors investigate the influence of the heating rate of the preheating process (4 or 10 °C/min) on the crystallization, surface morphology, and optical properties of sol–gel derived ZnO thin films. The ZnO sol was synthesized by dissolving zinc acetate dehydrate in ethanol, and then adding monoethanolamine. The as-coated films were preheated at 300 °C for 10 min and annealed at 500 °C for 1 h in air ambiance. Experimental results indicate that the heating rate of the preheating process strongly affected the surface morphology and transparency of ZnO thin film. Specifically, a heating rate of 10 °C/min for the preheating process produces a preferred orientation along the (0 0 2) plane and a high transmittance of 92% at a wavelength of 550 nm. Furthermore, this study reports the fabrication of thin-film transistors (TFTs) with a transparent ZnO active channel layer and evaluates their electrical performance.

1. Introduction

Zinc oxide (ZnO) is a II–VI group, n-type direct bandgap semiconductor that possess some great characteristics, including a wide energy bandgap (3.3 eV) [1], large free exciton binding energy (60 mV), wide range resistivity (10^{-4} to 10^{12} Ω cm), high carrier mobility, high transparency at room temperature, and good photoelectric, piezoelectric, and thermoelectric properties. As a result, ZnO has been used in numerous applications, including UV detectors, gas sensors, thin-film transistors, photovoltaic devices, piezoelectric transducers, surface acoustic wave (SAW) devices, and thermoelectric devices [2,3]. This is primarily due to its chemical stability, high carrier mobility, and lower photosensitivity than that of hydrogenated amorphous silicon (a-Si:H) thin films, which typically serves as the active channel layer in a typical TFT array for driving liquid crystal display (LCD) [4] and organic light-emitting device (OLED) display [5]. Recently, ZnO-based transparent thin films have also attracted attention for applications in transparent electronics, including thin-film solar cells, transparent thin-film transistors [6,7], and transparent electronic circuits [8,9].

ZnO-based thin films have been prepared by various vacuum deposition techniques and solution-based deposition processes [3]. Solution-based deposition processes offer a simple, low cost, and large area thin-film coating alternative to vacuum deposition techniques. Using the solution process to form oxide semiconductors may improve the manufacturing throughput of microelectronic and optoelectronic devices since it enable a direct pattern technique. Examples of this technique includes inkjet printing [10,11], microcontact printing [12,13], and reel to reel printing [14].

The sol–gel method not only enables easy fabrication of a large area thin film at a low cost, but also easily controls over the film composition and uniformity of thickness. Previous reports indicate that solution processes usually produce ZnO films with preferential crystal orientation, which could be important for efficient charger transport and could profoundly influence the mobility of field effect transistors (FETs) [15,16]. The polycrystalline ZnO thin films with *c*-axis orientation prepared by the sol–gel process that depends on the sol concentration [17–19], heat-treatment conditions [1,17,20–24], substrates used [25–27], and film thickness [20,28]. In the present study, transparent and semiconducting ZnO thin films were prepared by the sol–gel method using a spin-coating technique. This study also investigates the effect of the heating rate of the preheating procedure on the crystallization, microstructure, and optical properties of ZnO thin films. Finally, this study reports the fabrication of TFTs with a ZnO active channel layer and evaluates their electrical characteristics.

2. Experimental procedures

To synthesize the ZnO sol, zinc acetate dehydrate ($Zn(CH_3COO)_2{\cdot}2H_2O$) was first dissolved in an ethanol solvent, and then monoethanolamine (MEA) was added to

* Corresponding author. Tel.: +886 4 24517250x5312; fax: +886 4 24510014.
E-mail address: cytsay@fcu.edu.tw (C.-Y. Tsay).

0925-8388/$ – see front matter © 2010 Elsevier B.V. All rights reserved.
doi:10.1016/j.jallcom.2010.01.100

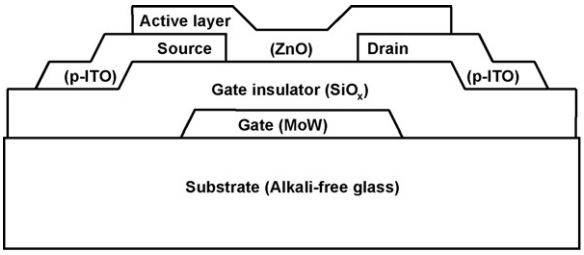

Fig. 1. Schematic diagram of the bottom-gate structure ZnO-TFT.

the solution as a stabilizer. We used ethanol, a low boiling point and non-toxicity solvent to synthesize un-doped ZnO sols. The molar ratio of zinc ions to MEA in the as-prepared sols was maintained at 1.0, and the zinc ions concentration was controlled at 0.75 mole/L. The complex solution was stirred for 2 h at 60 °C to yield a transparent, homogenous, and stable sol. A ZnO sol served as the coating solution after aging for 2 days at room temperature. Un-doped ZnO thin films were coated onto pre-cleaned glass substrates (NEG OA-10 alkali-free glass, with a size of 50 mm × 50 mm) using the spin-coating technique at a speed of 3000 rpm for 20 s. Each as-coated film was heated from room temperature to 300 °C (at a heating rate of 4 or 10 °C/min) and then maintained at 300 °C for 10 min. The samples were then heated to 500 °C (at a heating rate of 4 °C/min) and then maintained at 500 °C for 1 h in a tube furnace in air ambiance.

The crystal structures of sol–gel derived ZnO thin films were examined by X-ray diffractometry (XRD, MAC Science MXP3, Japan). Plane views of ZnO films and cross-sectional views of the ZnO-TFT device were observed using a field-emission scanning electron microscope (FE-SEM, Hitachi S-4800, Japan). The films' surface morphologies and surface roughness levels were examined by using a multimode scanning probe microscope (SPM, Digital Instrument NS4/D3100CL/MultiMode, Germany). The optical transmittance spectra of ZnO thin films were examined with a UV–VIS spectrophotometer (Shimadzu UV-1601, Japan). Sheet resistance was measured at room temperature using a high resistivity meter (Mitsubishi Chemical Corp. MCP-HT450, Japan).

The experiments in this study used a ZnO thin film with a flat free surface, good crystallinity, and high optical transparency for the active channel layer of TFTs application. The ZnO-TFTs were fabricated with a bottom-gate structure using a hybrid manufacturing process that combined microelectronic fabrication technology and the sol–gel spin-coating method. Fig. 1 shows the configuration of a bottom-gate TFT with the ZnO channel layer, and the following section describes the ZnO-TFT fabrication procedure. A molybdenum–tungsten (MoW) alloy thin film with a thickness of 100 nm was first sputtered onto a glass substrate, and then patterned by a photolithography process to produce the bottom-gate electrode. A 200 nm thick silicon oxide (SiO_x) film, prepared by plasma-enhanced chemical vapor deposition (PECVD), served as the gate insulator. A 100 nm thickness of indium tin oxide (ITO) thin film was deposited onto the gate insulator (SiO_x) and then patterned by a conventional photolithography process into a source and a drain electrode. The channel length and width of the TFT were offset at 500 and 40 μm, respectively. Finally, a ZnO semiconductor thin film was spin-coated onto the MoW/SiO_x/ITO multilayer stack and patterned by photolithography and wet etching processes into the desired island pattern to complete the ZnO-TFT. The current–voltage (I–V) characteristics of ZnO-TFT were measured in a shielding box using a semiconductor parameter analyzer (HP 4155B, USA).

3. Results and discussion

The crystallinity and crystal structure of sol–gel derived ZnO thin films were identified by X-ray diffraction. Fig. 2 shows the XRD patterns of ZnO thin films prepared at different preheating process heating rates (4 or 10 °C/min). These patterns correspond to six diffraction peaks of polycrystalline ZnO at (1 0 0), (0 0 2), (1 0 1), (1 0 2), (1 1 0) and (1 0 3) planes (JCPDS 36-1451). This result reveals that ZnO gel films preheated at 300 °C and annealed at 500 °C have a hexagonal wurzite structure. Note that the X-ray diffractograph of ZnO film prepared with a fast-heating rate (10 °C/min) in the preheating process shows a high (0 0 2) diffraction peak intensity (curves (ii) in Fig. 2 and insert of Fig. 2), namely the ZnO film exhibits preferential orientation along the (0 0 2) plane. Previous studies indicate that ZnO films with preferential crystal orientation were effective in reducing film resistivity [29] and assisting charge transport in the active channel layer of TFTs [15,16]. Some ZnO films preparation conditions and parameters affect the crystal orientation of sol–gel derived ZnO films. These parameters include sol concentration, heat-treatment temperature, post-annealing conditions, film thickness and substrate used. Ohya et al. indicated that the nucleation step determines the crystallization of metal oxide films [30]. Furthermore, Jiwei et al. proposed ZnO films with a (0 0 2) orientation because of their growth characteristics are kinetically preferred. The feature inferred the highest density of Zn atoms is found along the (0 0 2) plane [25].

This study estimates the average crystallite size (d) of ZnO films using Scherrer's formula. Table 1 summarizes the microstructure and other properties of ZnO thin films. The average crystallite size of ZnO thin films prepared with 4 or 10 °C/min heating rates for the preheating process were 8.9 and 11.5 nm. This shows that a thin-film prepared with a fast-heating rate in the preheating process exhibited larger average crystallite size due to its higher crystallinity. The lattice parameters of the a- and c-axes were calculated using $a = \lambda/\sqrt{3}\sin\theta$ and $c = \lambda/\sin\theta$, where $\lambda = 1.5406$ Å. The calculations in Table 1 shows two samples with the same a-axis length of 3.246 Å which is very close to the a-axis lattice parameter of

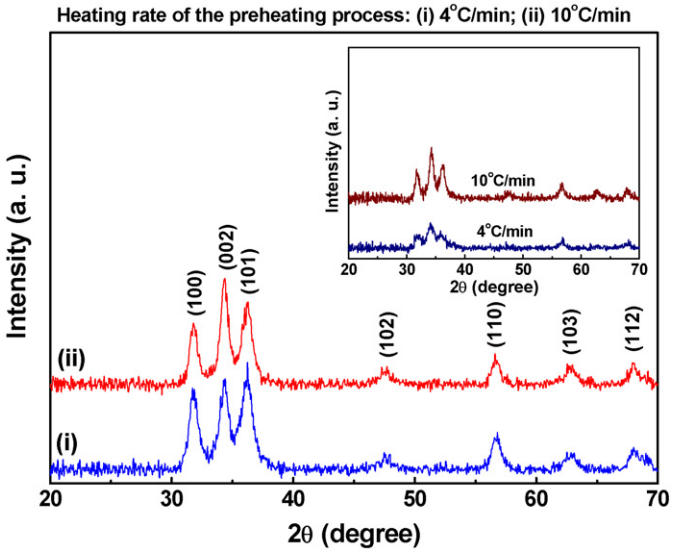

Fig. 2. X-ray diffraction patterns of ZnO thin films, which were preheated at 300 °C for 10 min and annealed at 500 °C for 1 h. The insert shows the XRD patterns of sol–gel derived ZnO thin films preheated at 300 °C for 10 min.

Table 1
Microstructure, surface roughness and visible transmittance for sol–gel derived ZnO thin films.

Heating rate for preheating process (°C/min)	Average crystallite size (nm)	Lattice parameters (Å)		Strain (%)	RMS roughness (nm)	Transmittance[a] (%)
		a-axis	*c*-axis			
4	8.9	3.246	5.222	0.288	10.9	60.3
10	11.5	3.246	5.218	0.211	7.1	92.0

[a] Only transmittances at the wavelength of 550 nm were presented in this table.

ZnO crystal (JCPDS 36-1451), but the *c*-axis lengths are great than that.

This study also uses the *c*-axis lattice parameter to estimate the film strain (ε_{zz}) along the *c*-axis given by the following formula [31], (1):

$$\varepsilon_{zz} = \frac{c - c_0}{c_0} \times 100\%, \quad (1)$$

where, c is the lattice parameter of ZnO films calculated from XRD data and c_0 is the unstrained lattice parameter of ZnO. According to the above formula, the positive value of ε_{zz} represents tensile strain while a negative value represents compressive strain. The estimations presented in Table 1 show that the strain in sol–gel derived ZnO films is tensile, and that films prepared with a heating rate of 10 °C/min in the preheating process exhibit lower magnitude tensile strain than those samples prepared with a the heating rate of 4 °C/min. The tensile strain might due to a thermal mismatch between the ZnO film and the glass substrate [27].

Surface micrograph analysis shows the influence of the heating rate of the preheating process on ZnO thin films (Fig. 3). A plane-view SEM image of the ZnO film prepared with a heating rate of 4 °C/min exhibits fiber-like streaks (Fig. 3(a)). However, ZnO films prepared with a heating rate of 10 °C/min exhibit improved surface flatness (Fig. 3(b)). In previous studies [32,33], we reported that the surface of sol–gel derived ZnO films with fiber-like stripes or wrinkles induced a shortage of OR (hydroxyl or alkoxy) groups in the ZnO sol. Thus, a relatively smooth surface can be obtained when the starting materials provide enough OR groups. The present study demonstrates that adjusting the heating rate of the preheating process obviously improved the surface flatness and roughness. The rate of the heterogeneous nucleation typically reaches a maximum and the driving force for crystallization is higher at low temperature [34]. On the other hand, the decomposition behavior played an important role in the crystallization and orientation of the ZnO films. When it was heated for a relatively short time (quick evaporation for a ZnO sol), which might provide fine size crystal nucleus and a high quality film was obtained.

SPM images show that increasing the heating rate from 4 to 10 °C/min improved the surface morphologies of the films (Fig. 4). Fig. 4(a) further shows that plicate structure that cause to unflatness of surface. Table 1 presents the values of RMS roughness of

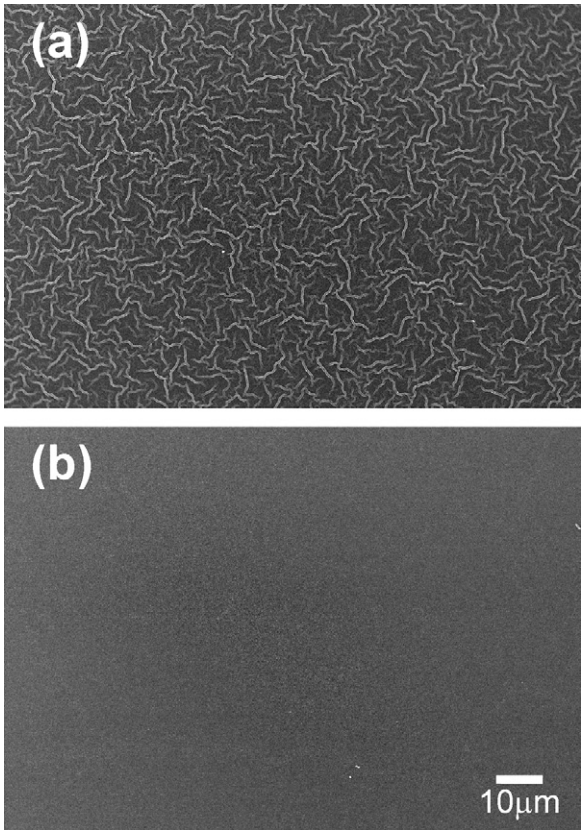

Fig. 3. Plane-view SEM micrographs of ZnO thin films: heating rate of the preheating process at (a) 4 °C/min and (b) 10 °C/min.

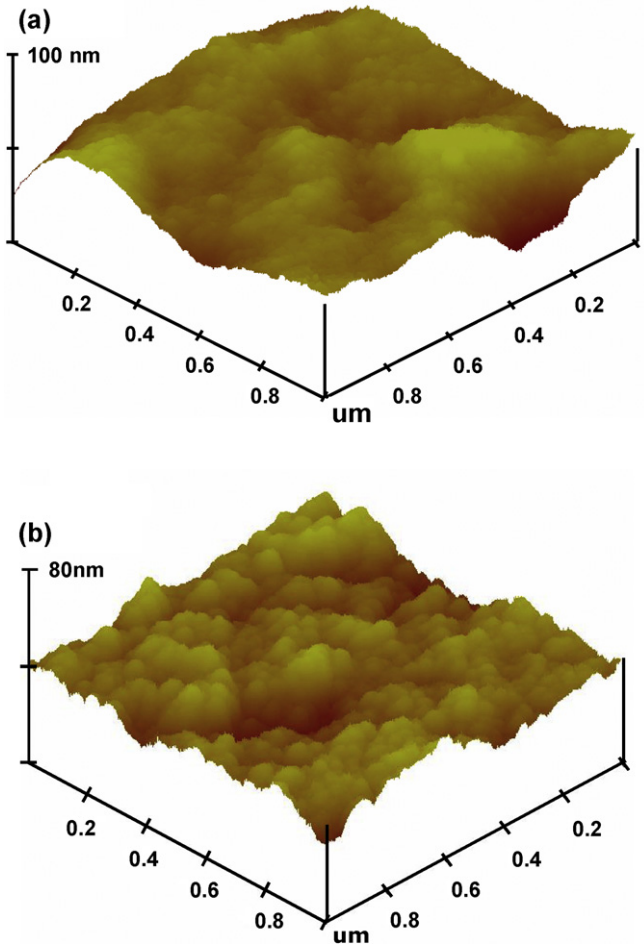

Fig. 4. SPM images of ZnO thin films: heating rate of the preheating process at (a) 4 °C/min and (b) 10 °C/min.

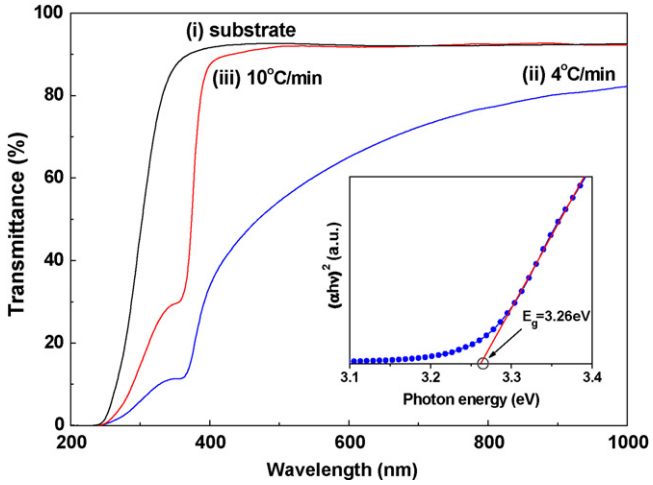

Fig. 5. Optical transmittance spectra of sol–gel derived ZnO thin films with different heating rates in the preheating process. The insert shows the plot of $(\alpha h\nu)^2$ versus photon energy of ZnO thin films prepared with a heating rate of 10 °C/min.

the ZnO films, indicating that RMS roughness decreased as the preheating process heating rate increased (Fig. 4(b)). The sample was heated at a rate of 10 °C/min exhibited better RMS roughness of 7.1 nm, representing a decrease of ~30% over the 4 °C/min sample.

Fig. 5 shows the optical transmittance spectra of ZnO films with wavelengths from 200 to 1000 nm. The sample prepared with a heating rate of 10 °C/min exhibits a sharp absorption edge at about 355 nm, and the film's transmittance between 550 and 1000 nm approaches the transmittance of the glass substrate. However, the sample prepared with a heating rate of 4 °C/min exhibits poor optical transmittance. Table 1 lists the transmittances for the 550 nm wavelength, indicating that the ZnO thin-film prepared with a heating rate of 10 °C/min exhibited a high transmittance of 92%. Surface morphology strongly affects the transparency of ZnO-based thin films [1]. In this study, the optical transmittance values are in good agreement with surface roughness values, which vary with the heating rate of the preheating process. Lee et al. [1] reported that sol–gel derived ZnO films possess a preferential orientation along the (0 0 2) plane, offering improved electrical and optical properties. The resistivity of a ZnO film can be calculated by multiplying the sheet resistances by the film thickness. Cross-sectional SEM micrograph (not shown) of the heating rate of 10 °C/min sample reveals film thickness is about 180 nm. Experimental results show that a ZnO film prepared with the heating rate of 10 °C/min has a sheet resistance of $4.8 \times 10^8\ \Omega/\square$. Thus, film's resistivity is $8.6 \times 10^4\ \Omega$ cm.

The optical transmittance spectrum of a ZnO thin-film prepared by a vacuum deposition technique should vanish in the UV region. However, this study shows that an absorption tail in the near UV region was observed for transmittance spectra of the as-prepared films. According to Tauc et al.'s study [35] the absorption edge spectrum can be separated into three distinct regions. The first is the weak absorption tail region, the second is the exponential edge region, and the third is the high absorption region [36]. In the present study, optical transmittance spectra in the near UV region did not display high absorption characteristics. This may be attributed to poor crystallinity in the sol–gel derived ZnO thin films.

The optical bandgap of a direct-semiconductor can be obtained by analyzing the absorption edge and applying the Tauc model [35],

$$(\alpha h\nu) = A(h\nu - E_g)^{1/2}, \tag{2}$$

where α is the absorption coefficient, $h\nu$ is the photon energy, A is a constant and E_g is the optical bandgap. The absorption coefficient (α) is directly related to the transmittance (T) and film thickness

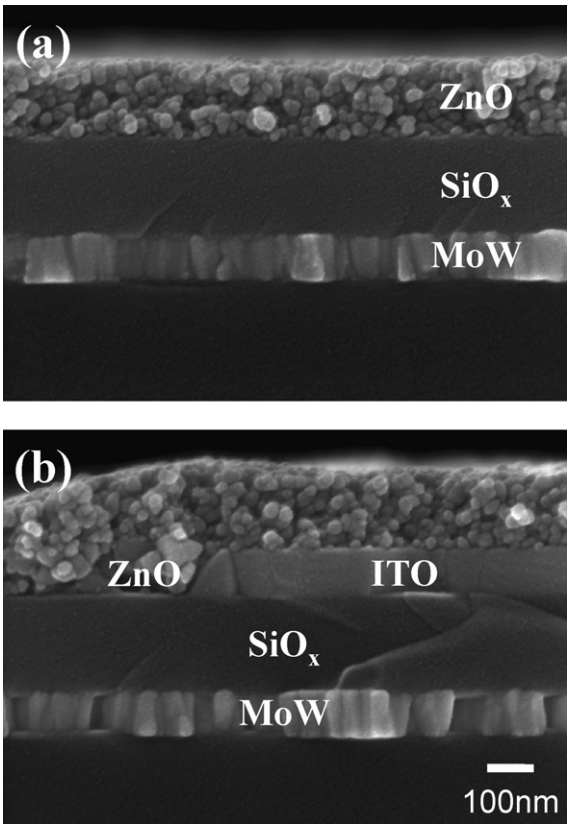

Fig. 6. Local cross-sectional view of ZO-TFT: (a) the active channel region and (b) the drain electrode region.

(d), which can be calculated using the following formula,

$$T = B\ \exp(-\alpha d), \tag{3}$$

where the constant B is approximately unity. The optical bandgap of a ZnO film prepared with a heating rate of 10 °C/min was determined by extrapolating the straight section for the plot of $(\alpha h\nu)^2$ versus the photo energy (insert of Fig. 5). The E_g value of 3.26 eV is similar to previous reports [37,38], but a little smaller than that of ZnO crystal (3.3 eV) [1]. The bandgap difference between the thin film and crystal is due to the grain boundaries and imperfections of the polycrystalline thin films [21].

The study analyzes a ZnO thin film with better performance, *i.e.*, with a flat film surface and high optical transparency, based on the above discussed characterization results for application as the active channel layer in a TFT. The study also evaluates the ZnO-TFT's current–voltage (I–V) characteristics. Fig. 6 shows two cross-sectional views of a ZnO-TFT. These images clearly indicate that the active channel layer exhibits a granular structure and the film is about 180–185 nm thick (Fig. 6(a)). A polycrystalline ZnO semiconductor film was successfully deposited on the MoW/SiO_x/ITO multilayer stack and well covered with ITO electrode and SiO_x gate insulator (Fig. 6(b)). There were no voids or pores in or between the SiO_x/ZnO and ITO/ZnO interfaces.

Fig. 7(a) shows the drain current–drain voltage (I_D–V_D) curves of a ZnO-TFT indicates that the TFT operates as an n-channel transistor. Fig. 7(a) also further shows that the drain current increases with the positive gate bias, the slope of each I_D curve is flat, and the drain current saturation is in the large V_D region. Fig. 7(b) shows the $\log(I_D)$–V_G and $\log(I_G)$–V_G curves for the same device. The transfer characteristic ($\log(I_D)$–V_G curve) was measured at a fixed drain voltage (V_D) of 40 V. The $\log(I_D)$–V_G curve reveals the off current is 10^{-11} A (at $V_G = -38$ V) and the on-to-off current ratio is

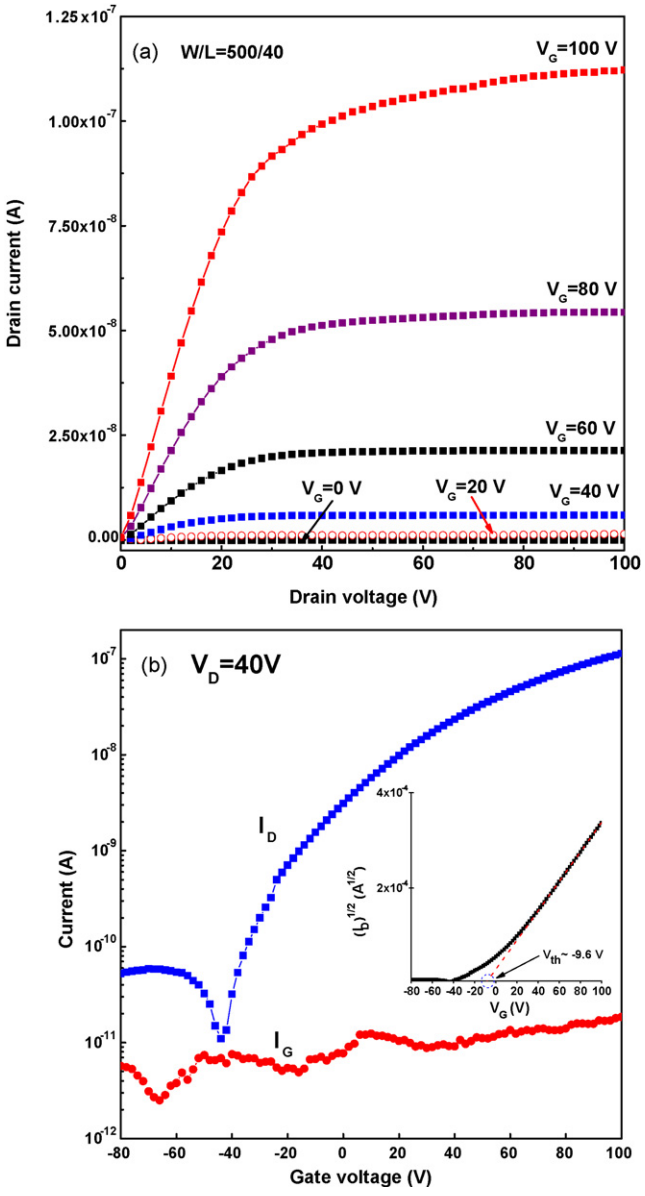

Fig. 7. (a) I_D–V_D curves (output characteristics); (b) log(I_D)–V_G (transfer characteristic) and log(I_G)–V_G curves of ZnO-TFT. The insert shows the threshold voltage (V_{th}) defined by fitting a straight line, and then intercepting the x-axis of the $(I_D)^{1/2}$–V_G curve.

about 1.0×10^4. From Fig. 7(b), one can observe that the gate leakage current (I_G) slightly increased as the measured gate voltage increased. The magnitude of I_G was below 2×10^{-11} A; therefore, the PECVD-grown SiO_x was usefully utilized as the gate insulator in this transistor. The insert of Fig. 7(b) is a $(I_D)^{1/2}$–V_G plot. The threshold voltage (V_{th}) of the transistor was derived from the $(I_D)^{1/2}$–V_G plot. By fitting a straight line and then intercepting the x-axis, a V_{th} of −9.6 V can be obtained. This result implies that the ZnO-TFT operates in the depletion mode.

4. Conclusions

Transparent semiconductor ZnO thin films were successfully prepared by the sol–gel method using a spin-coating technique. The as-deposited films exhibited a hexagonal wurtzite structure after annealing at 500 °C in air ambiance for 1 h. Increasing the heating rate of the preheating process from 4 to 10 °C/min obviously improved transparency in the visible range, decreased the surface roughness, and reduced strain for ZnO thin films. In the present study, ZnO thin films formed at a heating rate of 10 °C/min in the preheating process exhibited high optical transmittance of 92% and a resistivity of $8.6 \times 10^4\ \Omega$ m. The ZnO transparent semiconductor thin film could serve as the active channel layer of TFTs. The ZnO-TFT exhibited in n-channel depletion mode characteristic with a threshold voltage and on/off current ratio of −9.6 V and 1.0×10^4, respectively.

Acknowledgment

The authors gratefully acknowledge the financial support by the Taiwan TFT-LCD Association (TTLA) under Contract No. A643TT1000-S21.

References

[1] J.H. Lee, K.H. Ko, B.O. Park, J. Cryst. Growth 247 (2003) 119.
[2] S.J. Pearton, D.P. Norton, K. Ip, Y.W. Heo, T. Steiner, J. Vac. Sci. Technol. B 22 (2004) 932.
[3] S.M. Lukas, L.M.D. Judith, Mater. Today 10 (2007) 40.
[4] T. Hirao, M. Furuta, T. Hiramatsu, T. Matsuda, C. Li, H. Furuta, H. Hokari, M. Yoshida, H. Ishii, M. Kakegawa, IEEE Trans. Electr. Dev. 55 (2008) 3136.
[5] S.-H.K. Park, C.-S. Hwang, M. Ryu, S. Yang, C. Byun, J. Shin, J.-I. Lee, K. Lee, M.S. Oh, S. Im, Adv. Mater. 21 (2009) 678.
[6] E. Fortunato, P. Barquinha, A. Pimentel, A. Gonçalves, A. Marques, L. Pereira, R. Martins, Adv. Mater. 17 (2005) 590.
[7] H.C. Cheng, C.F. Chen, C.Y. Tsay, Appl. Phys. Lett. 90 (2007) 012113.
[8] R.E. Presley, D. Hong, H.Q. Chiang, C.M. Hung, R.L. Hoffman, J.F. Wager, Solid State Electron. 50 (2006) 500.
[9] M. Ofuji, K. Abe, H. Shimizu, N. Kaji, R. Hayashi, M. Sano, H. Kumomi, K. Nomura, T. Kamiya, H. Hosono, IEEE Electron Dev. Lett. 28 (2007) 273.
[10] S.T. Meyers, J.T. Anderson, C.M. Hung, J. Thompson, J.F. Wager, D.A. Keszler, J. Am. Chem. Soc. 130 (2008) 17603.
[11] J.J. Schneider, R.C. Hoffmann, J. Engstler, O. Soffke, W. Jaegermann, A. Issanin, A. Klyszcz, Adv. Mater. 20 (2008) 3383.
[12] H.J. Lim, D.Y. Lee, Y.J. Oh, Sens. Actuators A: Phys. 125 (2006) 405.
[13] T.L. Breen, P.M. Fryer, R.W. Nunes, M.E. Rothwell, Langmuir 18 (2002) 194.
[14] Y.G. Chang, S.H. Nam, N.K. Kim, Y.H. Kook, J. Kim, S.S. Yoo, C.D. Kim, I. Kang, I.J. Chung, SID 08 Digest, 2008, pp. 637.
[15] C.S. Li, Y.N. Li, Y.L. Wu, B.S. Ong, R.O. Loutfy, J. Phys. D: Appl. Phys. 41 (2008) 125102.
[16] B.S. Ong, C. Li, Y. Li, Y. Wu, R. Loutfy, J. Am. Chem. Soc. 129 (2007) 2750.
[17] Y.S. Kim, W.P. Tai, S.J. Shu, Thin Solid Films 491 (2005) 153.
[18] M. Dutta, S. Mridha, D. Basak, Appl. Surf. Sci. 254 (2008) 2743.
[19] S. O'Brien, L.H.K. Koh, G.M. Crean, Thin Solid Films 516 (2008) 1391.
[20] M. Ohyama, H. Kozuka, T. Yoko, Thin Solid Films 306 (1997) 78.
[21] D. Bao, H. Gu, A. Kuang, Thin Solid Films 312 (1998) 37.
[22] H. Li, J. Wang, H. Liu, C. Yang, H. Xu, X. Li, H. Cui, Vacuum 77 (2004) 57.
[23] M.W. Zhu, J. Gong, C. Sun, J.H. Xia, X. Jiang, J. Appl. Phys. 104 (2008) 073113.
[24] D. Raoufi, T. Raoufi, Appl. Surf. Sci. 255 (2009) 5812.
[25] Z. Jiwei, Z. Liangying, Y. Xi, Ceram. Int. 26 (2000) 883.
[26] S. Chakrabarti, D. Ganguli, S. Chaudhuri, Mater. Lett. 58 (2004) 3952.
[27] R. Ghosh, D. Basak, S. Fujihara, J. Appl. Phys. 96 (2004) 2689.
[28] M.H. Aslan, A.Y. Oral, E. Menşur, A. Gül, E. Başaran, Solar Energy Mater. Solar Cells 82 (2004) 543.
[29] M. Ohyama, H. Kozuka, T. Yoko, J. Am. Ceram. Soc. 81 (1998) 1622.
[30] Y. Ohya, H. Saiki, T. Tanaka, Y. Takahashi, J. Am. Ceram. Soc. 79 (1996) 825.
[31] H.C. Ong, A.X.E. Zhu, G.T. Du, Appl. Phys. Lett. 80 (2002) 941.
[32] C.Y. Tsay, H.C. Cheng, Y.T. Tung, W.H. Tuan, C.K. Lin, Thin Solid Films 517 (2008) 1032.
[33] C.Y. Tsay, M.C. Wang, S.C. Chang, J. Electron. Mater. 38 (2009) 1962.
[34] S. Fujihara, C. Sasaki, T. Kimura, Appl. Surf. Sci. 180 (2001) 341.
[35] J. Tauc, R. Grigorovici, A. Vancu, Phys. Stat. Sol. 15 (1966) 627.
[36] E.Ş. Tüzemen, S. Eker, H. Kavak, R. Esen, Appl. Surf. Sci. 255 (2009) 6195.
[37] G. Srinivasan, J. Kumar, J. Cryst. Growth 310 (2008) 1841.
[38] F.K. Shan, G.X. Liu, W.J. Lee, G.H. Lee, I.S. Kim, B.C. Shin, Y.C. Kim, J. Cryst. Growth 277 (2005) 284.